Evolutionary Biology
https://doi.org/10.1007/s11692-020-09515-9

RESEARCH ARTICLE

Interrelations Between the Cranium, the Mandible and Muscle Architecture in Modern Domestic Dogs

Colline Brassard[1,2] · Marilaine Merlin[1] · Claude Guintard[3,4] · Elodie Monchâtre-Leroy[5] · Jacques Barrat[5] · Cécile Callou[2] · Raphaël Cornette[6] · Anthony Herrel[1]

Received: 17 March 2020 / Accepted: 7 September 2020

Abstract

Many studies have attested to the consequences of the recent and intense artificial selection on the morphological variability of the cranium and mandible in domestic animals. However, the functional relations of the cranium with other constituents of the masticatory apparatus (the mandibles and the adductor muscles) have rarely been explored. Previous work has demonstrated strong relationships between the overall shape of the mandible and muscle data, however, drastic artificial selection in dogs has led to frequent malocclusions, suggesting a possible decoupling between the cranium and the mandible. Moreover, the more complex role of the cranium suggests that it is likely less impacted by, and correlated with, the architecture of the jaw muscles than the mandible. We explored the covariations between cranial and mandibular shape and between cranial shape and the masticatory muscle architecture. Shape analyses were conducted on 58 dogs from various breeds and we used muscle data previously obtained from the dissection of 48 of these dogs. The shape of the cranium was quantified using 3D geometric morphometric approaches. Principal component analyses (PCA) and two-block partial least square analyses (2B-PLS) were used to quantify the variations in cranial shape and the covariations with mandible shape and muscle architecture, respectively. Interestingly, our results reveal strong covariations between cranial shape and mandibular shape and between cranial shape and masticatory muscles mass or physiological cross-sectional area, irrespective of whether size is taken into account or not. We conclude that the drastic artificial selection in domestic dogs has not tainted the integrity of the jaw system, which reinforces previous assumptions hypothesising that phenotypic variability in dogs may be limited by developmental factors.

Keywords Dog · Skull · Masticatory system · Jaw muscle architecture · Domestication · Geometric morphometrics

Introduction

Many studies have focused on the modularity and integration of the skull in carnivores and have attested to the consequences of domestication on the morphological variability

Colline Brassard and Marilaine Merlin are co-first authors.

Electronic supplementary material The online version of this article (https://doi.org/10.1007/s11692-020-09515-9) contains supplementary material, which is available to authorized users.

✉ Colline Brassard
colline.brassard@mnhn.fr

[1] UMR 7179 Mécanismes Adaptatifs et Evolution (CNRS, MNHN), Muséum national d'Histoire naturelle, 55 rue Buffon, Paris, France

[2] Archéozoologie, archéobotanique : sociétés, pratiques et environnements (AASPE), Muséum national d'Histoire naturelle, CNRS, 57 rue Cuvier, CP5575005 Paris, France

[3] Laboratoire d'Anatomie comparée, Ecole Nationale Vétérinaire, de l'Agroalimentaire et de l'Alimentation, Nantes Atlantique – ONIRIS, Nantes Cedex 03, France

[4] GEROM, UPRES EA 4658, LABCOM ANR NEXTBONE, Faculté de santé de l'Université d'Angers, Angers, France

[5] ANSES, Laboratoire de la rage et de la faune sauvage, Station expérimentale d'Atton, Malzéville, France

[6] UMR 7205, Institut de Systématique, Evolution, Biodiversité (CNRS, MNHN, UPMC, EPHE), Muséum national d'Histoire naturelle, Paris, France

Published online: 18 September 2020

of the cranium and mandible (Drake and Klingenberg 2008, 2010; Curth et al. 2017; Curth 2018; Machado et al. 2018; Selba et al. 2019). Over the last century, drastic artificial selection has led to huge variability in dog morphotypes (Drake and Klingenberg 2010). Domestic dogs are thus a good model to study the functional consequences of skull shape variation in canids. The great morphological diversity in the cranium of dogs raises questions, however, about the interplay between the jaw muscles and the bones of the head given that bones are known to model and remodel in relation to external forces like muscle forces (Frost 2001, 2003; Schoenau 2005; Sharir et al. 2011; Brotto and Bonewald 2015). Yet, to date our understanding of the interrelationships between bones, muscles, and bite force in dogs remains incomplete (but see Ellis et al. 2008, 2009; Kim et al. 2018; Brassard et al. 2020a, b). Historically, selective breeding was based on the requirement for specific morphological traits or performance without regard for genetic health and integrity. This intensive selection leads to frequently distorted dentitions, particularly in brachycephalic breeds (Bell 1965). The cranium is often too short (maxillary brachygnathism, e.g. in the Bulldog) or too long (mandibular brachygnathism, e.g. in the Bull terrier; Milella 2009) to accommodate all the teeth. These frequent malocclusions well illustrate the possible functional decoupling between the cranium and the mandible, and possibly between the jaw and its associated musculature.

Because dogs are no longer submitted to natural selection, one would expect a disruption in the functional integrity of the jaw. Interestingly, previous results have shown that the shape of the mandible strongly covaries with the architecture of the adductor muscles (Brassard et al. 2020a). This suggests that strong functional connections still exist in the head of dogs, despite intense artificial selection. However, whereas the mandible is involved in a single function (chewing) the cranium faces many other functional challenges as it also protects the sensory organs and the brain, for example. Moreover, selection for aesthetics reasons has often focused specifically on morphological traits of the cranium rather than on the mandible. As a consequence, it is possible that the functional links between the mandible and the cranium, and between jaw muscles and cranial shape, may be impacted by this selection. We thus expect the shape of the cranium to covary relatively little with mandible shape and to be less strongly driven by variation in jaw muscle volume or intrinsic muscle strength than the mandible.

The aims of the present study were to (1) explore the variability in cranial shape in a range of dogs of various sizes and morphotypes, (2) to test whether the shape of the cranium covaries with that of the mandible despite frequent malocclusion due to artificial selection, and (3) to test whether the shape of the cranium is related to the architecture of the jaw muscles and whether this covariation is less important than for the mandible. We predict that strong artificial selection will have resulted in a functional decoupling between the cranium and the mandible, resulting in little covariation between the shape of the cranium and that of the mandible, and possibly in a lower integration between the jaw muscle architecture and the shape of the cranium than between muscle architecture and mandible shape.

Materials and Methods

Materials

In this study, we studied the skull of 58 dogs from various breeds (see Table S1 for a complete list of the specimens used in the analyses). The cadavers were collected from a veterinary school (ONIRIS, Nantes, France) and from a wildlife disease study centre (ANSES in Nancy, France). Dogs were unlikely to be pure bred (membership to a standard was not known). Those that were morphologically close (in shape and color) to existing breeds were assigned as such to provide context for further discussions (see Table 1). Additionaly, for visualisation and discussion purposes, dogs were categorised into brachycephalic, mesocephalic or dolichocephalic, based on the cephalic index (CI = skull width/skull length * 100; Roberts et al. 2010). Skull length was measured from the anterior tip at the end of the suture of the nasal bones (landmark 2, Fig. 1) to the most posterior point on the occipital protuberance (landmark 14, Fig. 1). Skull width was measured between the two zygomatic arches (landmark 37 and the symmetric landmark to the sagittal plane, Fig. 1). Dogs with a cephalic index less than 0.70 were considered brachycephalic and dogs with an index less than 0.60 were considered dolichocephalic. The dogs with an index between 0.60 and 0.70 were considered mesocephalic. The boundary between groups was chosen to ensure that the three groups are similar in size, but specimens within the same breed can be classified in two adjacent morphotypes. Additionaly, the specimens were classified into four age groups depending on the degree of closure of the cranial sutures and dental eruption patterns. Group 'A' corresponds to the youngest individuals with permanent teeth still erupting (4–6 months according to Barone 2010), group 'B' to individuals with the sphenobasilar suture still open (< 8–10 months for the dog according to Barone 2010), group 'D' to dogs with a closed interfrontal suture and worn dentures (> 3–4 years), and group 'C' to intermediate adults (from 10 months to 3 years). We chose to keep the youngest individuals in our analyses to increase the morphological variability in the sample, but most of the dogs are adults or old adults. We did not include geriatric dogs in our sample.

Table 1 List of the specimens used in this study

Estimated breeds	Age groups				Morphotype	N		
	Juvenile	Young	Adult	Old		Cranium and mandible	PCSA	Mass
American Staffordshire terrier			1		Brachycephalic	1	1	1
Beagle	1	2	15	3	Mesocephalic	20	10	10
Belgian shepherd—Tervueren				2	1 mesocephalic 1 dolichocephalic			
Border collie			1	1	Dolichocephalic	2	2	2
Boxer				2	Brachycephalic	2	2	2
Bulldog			1	1	Brachycephalic	2	2	2
Bull terrier	1				Mesocephalic	1	1	1
Cane Corso			1		Brachycephalic	1	1	1
Cavalier King Charles Spaniel			1		Brachycephalic	1	1	1
Chihuahua				1	Brachycephalic	1	1	1
Collie				1	Dolichocephalic	1	1	1
Continental Toy Spaniel Papillon			1		Brachycephalic	1	1	1
Dachshund			1		Dolichocephalic	1	1	1
Deerhound				1	Dolichocephalic	1	1	1
Dobermann				1	Dolichocephalic	1	1	1
Fox terrier			1		Mesocephalic	1	1	1
German shepherd				1	Dolichocephalic	1	1	1
Golden retriever			1		Dolichocephalic	1	1	1
Husky			1		Dolichocephalic	1	1	1
Leonberger			1		Dolichocephalic	1	1	1
Mastiff			1	1	Mesocephalic	2	2	2
Pitbull				1	Brachycephalic	1	1	1
Rottweiler			2		Brachycephalic	2	2	2
Shetland sheepdog			1		Dolichocephalic	1	1	1
Non-estimated breed			3	6	2 mesocephalic 5 dolichocephalic 2 brachycephalic	9	9	8
Total	2	2	33	22		58	48	47

N number of specimens, represented by both their mandible and cranium. Note that the number of individuals is different for the study of the covariation between the cranium and mandible shape, and between muscle data and cranial shape. Estimated breeds refer to the assignment of the breed for each dog

Muscle fiber lengths, pennation angles, masses and physiological cross-sectional areas (PCSAs) were quantified for 48 and 47 of these dogs, respectively (Brassard et al. 2020a). Pennation angles and $\log_{10}$-transformed muscle fiber lengths, masses and reduced physiological cross-sectional area (PCSA) were calculated for the digastric (Dig) and the adductor muscles: the M. masseter pars superficialis (MS), the M. masseter pars profunda (MP), the M. zygomaticomandibularis pars anterior (ZMA), the M. zygomaticomandibularis pars posterior (ZMP), the M. temporalis pars suprazygomatica (SZ), the M. temporalis pars superficial (TS), the M. temporalis pars profunda (TP), and the M. pterygoideus (P). Since the M. pterygoideus pars lateralis attaches to the condyle (that is the fulcrum system), it is more an anterior translator than an adductor muscle. However, it is very small (it represents less than 1% of the total muscle volume; Brassard et al. 2020a) and difficult to clearly distinguish from the M. pterygoideus pars medialis. Accordingly, we considered both muscles as a single muscle mass.

Landmarking

Shape analyses were conducted using geometric morphometrics. Landmark locations are provided in Fig. 1 and Table 2. Because the crania were often broken, and because cranial shape is easily described with a relatively small number of landmarks, contrary to the mandible, different methods were used for landmarking the cranium and mandible.

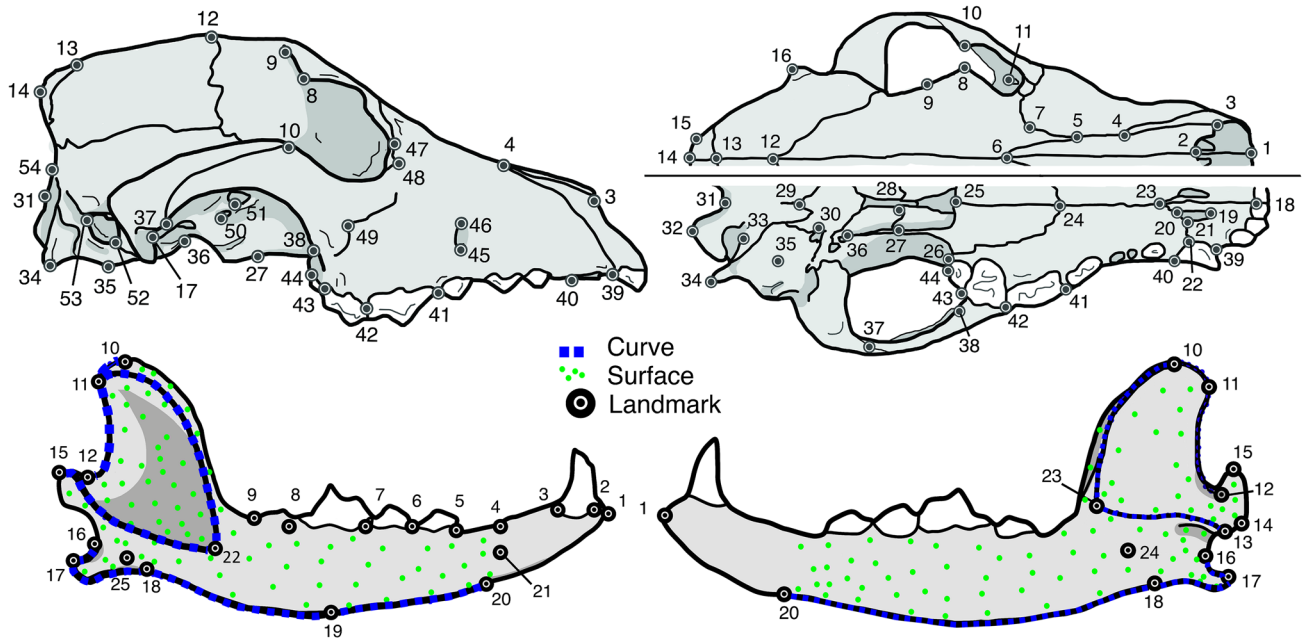

Fig. 1 Landmarks used in this study, illustrated in dorsal, lateral and ventral views of the cranium and mandible of a beagle. Anatomical landmarks are in black, landmarks on curves are in blue and surface landmarks are in green. We refer to Table 2 and Table S2 (Supplementary file 5) for the definitions of the landmarks on the cranium and mandible, respectively

To quantify cranial shape we recorded fifty-four 3D landmarks on one side using a MicroScribe MX (MicroScribe MX R", REVWARE). A mirror function was then applied to obtain the symmetrical landmarks relative to the sagittal plane using the function 'mirrorfill' from the package 'paleomorph'. This resulted in a total of 108 landmarks. For further visualisation of cranial shape, the cranium of a beagle (which shape is close to the mean shape of our sample) was photographed using a Nikon D5500 Camera (24,2 effective megapixels) with a 60 mm lens. One hundred and forty photographs were taken by turning around the dorsal and ventral views of the cranium (Fau et al. 2016). 3D models of the crania were obtained after merging the two sides, using the Agisoft PhotoScan software (© 2014 Agisoft LLC, 27 Gzhatskaya st., St. Petersburg, Russia).

The landmarks on the mandible were taken from a previous study (Brassard et al. 2020a). In brief, we obtained 3D reconstructions of the mandible using photogrammetry. To do so we used the same camera than the one mentioned above. One hundred photographs were taken by turning around the dorsal and ventral views of the mandible. A total of 400 landmarks (including 25 homologous anatomical landmarks, 190 sliding semilandmarks on curves and 185 sliding semilandmarks on the surface) were placed on the mandibles using the software Landmark, version 3.0.0.6 (© IDAV 2002–2005) (Wiley et al. 2005). A sliding semi-landmark procedure (Bookstein 1997; Gunz et al. 2005; Schlager 2012) was performed to obtain homologous landmarks. The 3D model of a beagle's right mandible (for the same reasons as stated above) was used to visualise variation in mandibular shape.

Shape Analyses with Geometric Morphometrics

Shape analyses were conducted using the packages 'Morpho' (version 2.7) and 'geomorph' (version 3.1.2) in R (version 3.6.0; 2019-04-26). All specimen were aligned, scaled and translated using a Generalized Procrustes Analysis (GPA—Rohlf and Slice 1990) using the function 'procSym' (Klingenberg et al. 2002; Gunz et al. 2005; Dryden and Mardia 2016). The theoric shape of the consensus of each GPA (on cranial or mandibular shapes) was obtained by deforming the reference beagle specimen to the mean shape of the GPA, using the function 'tps3d'. In order to perform analyses without size, we also obtained allometry-free shapes using the functions 'CAC' (Mitteroecker et al. 2004), and 'showPC'.

Principal component analyses (PCA) were performed based on the Procrustes coordinates using the function 'procSym'. We also performed a PCA on the allometry-free shapes using 'plotTangentSpace'. Visualisations at the minimum or maximum of the two first principal components were obtained using the functions 'plotTangentSpace', 'tps3d' and 'deformGrid3d'. We computed linear models to explain each PCA component by the size of the individuals. Sample sizes were too small and too different between sexes

Table 2 Definitions of the landmarks placed on the cranium and used in the geometric morphometric analyses, following the N.A.V. nomenclature

Landmark	Definition
1	Most rostral point of *Os incisivum*, between incisors I1 in dorsal view
2	Most rostral point of *Os nasale*, on the midline (*Sutura internasalis*)
3	Most rostral point on *Sutura nasoincisiva*
4	Point at the junction of *Os incisivum*, *Os nasale* and *Maxilla*
5	Point at the junction of *Os nasale*, *Maxilla* and *Os frontale*
6	Most rostral point of *Os temporale* and most caudal point of *Os nasale*, on the midline (*Sutura internasalis*)
7	Most posterior point of the *Maxilla* in dorsal view
8	Most lateral point of the *Processus zygomaticus* of *Os frontale*
9	Most medial point of the curvature corresponding to the *Linea temporalis*, most medial point at the postorbital constriction
10	*Processus frontalis* of *Os zygomaticum*
11	Most rostral point of the curvature of the lower edge of the *Fossa sacci lacrimalis*
12	Bregmatic fontanel, most medial point of the *Sutura coronalis*, on the midline
13	Most medial point on the *Sutura lambdoidea*
14	Inion, posterior end of *Os occipitale*
15	Point at the extreme convex curvature of the *Tuberculum nuchale*
16	Point at the extreme convex curvature of the *Crista supramastoidea*
17	*Fossa mandibularis*, on the *Sutura sphenoparietalis*
18	Central point of the *Sutura interincisiva* in ventral view, just posterior to the two incisors I1
19	Most rostral point of the *Fissura palatina*
20	Most caudal point of the *Fissura palatina*
21	Point on the *Fissura palatina* at the junction between *Os incisivum* and *Maxilla* in ventral view
22	Point between the *Canina* and the incisor I3 at the junction between *Os incisivum* and *Maxilla* in ventral view
23	Most rostral point of *Maxilla* in ventral view, on the midline
24	Most rostral point of the *Sutura palatomaxillaris*, on the midline
25	Most caudal point of *Os palatinum*, on the midline
26	Point near molar M2, on the *Sutura palatomaxillaris*
27	Ventral point on the *Sutura sphenopalatina*
28	Point on vomer, at the junction with *Os presphenoidale* (*Sutura vomerosphenoidalis*)
29	Most caudal point of the *Synchondrosis sphenooccipitalis*, on the midline
30	Most lateral point of the *Synchondrosis sphenooccipitalis*, rostrally to the *Bulla tympanica*
31	Most cranial point of the caudal curve of *Os occipitale* (*Foramen magnum*) in ventral view, on the midline
32	Most caudal point of the caudal curve of *Os occipitale* in ventral view
33	Point on the *Foramen lacerum*
34	*Processus paracondylaris*
35	Ventral tip of the *Bulla tympanica*
36	Most dorsal and caudal point of the curve of the *Foramen alare caudale*
37	Most ventral and posterior point at the junction of the *Pars squamosa* of *Os temporale* and *Os zygomaticum*, on the *Arcus zygomaticus*
38	Most caudal point at the junction between *Maxilla* and *Os zygomaticum*, near M2
39	Most cranial point of the alveolus of the *Canina*
40	Most caudal point of the alveolus of the *Canina*
41	Most cranial point of the alveolus of the upper carnassial P4
42	Point between the alveolus of P4 and M1
43	Point between the alveolus of M1 and M2
44	Most caudal point of *Maxilla* behind M2
45	Most dorsal point of the *Foramen infraorbitale*
46	Most ventral point of the *Foramen infraorbitale*
47	Point at the junction of *Maxilla*, *Os lacrimale* and *Os temporale*

Table 2 (continued)

Landmark	Definition
48	Point at the junction of *Maxilla*, *Os lacrimale* and *Os zygomaticum*
49	Most caudal point of curvature at the junction of *Maxilla* and *Os zygomaticum*
50	Most ventral and caudal point of the *Foramen alare rostrale*
51	Most ventral and caudal point of the *Fissura orbitalis*
52	Most rostral point of *Meatus acusticus externus* in lateral view
53	Most caudal point of *Meatus acusticus externus* in lateral view
54	Opisthion, dorsal and caudal border of the *Foramen magnum*, on the midline

We refer to Table S2 (Supplementary file 5) for the definitions of the landmarks on the mandible

(9 females and 23 males) and age groups (two juvenile and two young dogs only) to test for the effect of these variables (Tables 1, S1).

Relationships Between Cranial, Mandibular Shape and Muscle Data

To investigate the drivers of cranial and mandibular shape we performed non-parametric Procrustes ANOVA/regressions with permutation procedures on the shape coordinates and centroid size (of the cranium or mandible), residual muscle mass and PCSA data using the function 'procD.lm' with 1000 iterations (Goodall 1991; Anderson 2001; Anderson and Braak 2003; Collyer et al. 2015; Adams and Collyer 2016, 2017). We performed multiple and simple regressions (to better describe the amount of variation in shape explained by variation in a single explanatory variable) on the coordinates from the GPA (allometric shape) and on the coordinates of the allometry-free shape. We performed these analyses with the three main adductor complexes in order to increase statistical power: the masseter complex, the temporal complex, and the pterygoid complex. For each complex, fiber lengths were averaged while masses and PCSAs were summed. Data were $\log_{10}$-transformed. We used the 'shape.predictor' function and the 'Avizo 8.1.1.' software to visualize the effect of the variation in the PCSA of the temporal, masseter, and pterygoid muscles on the shape of the cranium and mandible.

Additionally, to test whether certain head-types differed significantly in muscle mass or PCSA for their size, we performed ANOVAs (function 'aov') and post-hoc tests (function 'TukeyHSD') to compare the residual muscle masses and muscle PCSAs for the three main adductor complexes between brachycephalic, mesocephalic and dolichocephalic dogs.

To understand the covariations between the shape of the cranium and that of the mandible and between cranial shape and the muscle data we performed two-block partial least squares analyses (2B-PLS) with the function 'pls2B' (Rohlf and Corti 2000). P-values (attesting to the significance of the covariations) were computed from 1000 permuted blocks. Because the dogs are from mixed breeds, we did not consider phylogeny (Parker et al. 2004) in our analyses. Because variation in the shape of the cranium and mandible and the muscle data is largely driven by size (Wayne 1986; Brassard et al. 2020a), we also quantified the covariation between residual muscle data and/or allometry-free shapes. Residual muscle data were calculated using the function 'lm', considering the $\log_{10}$-transformed centroid size of the cranium as our proxy of size. A total of thirteen 2B-PLS analyses were conducted: cranial shape—mandibular shape, allometry-free cranial shape—allometry-free mandibular shape, cranial shape—muscle mass, cranial shape—residual mass, allometry-free cranial shape—residual mass, cranial shape—PCSA, cranial shape—residual PCSA, allometry-free cranial shape—residual PCSA. Visualisations at the minimum or maximum of the PLS axes were obtained using the functions 'plsCoVar', 'tps3d' and 'deformGrid3D'. To compare PLS coefficients from this study and those from previous work (Brassard et al. 2020a), we calculated Z-scores using the function 'compare.pls'. Juveniles were excluded from the analyses of covariation between cranial and mandibular shape.

Results

We refer to the Supplementary file 6 for detailed results of the statistical analyses. Below we describe the main patterns only.

Variability in Cranial Shape

The first two axes of the PCA on cranial shape (Fig. 2a) represent 63.5% of the total variance (the first six axes explain 80% of the total variance). Linear models show that variation along PC1 is driven by variation in size (adjusted $R^2 = 0.23$, $P < 0.001$). PC2 is mostly related to variation in centroid size (adjusted $R^2 = 0.58$, $P < 0.001$). The first axis of the PCA with cranial shape (Fig. 2a) separates the brachycephalic (with short but wide crania) from the more dolichocephalic dogs

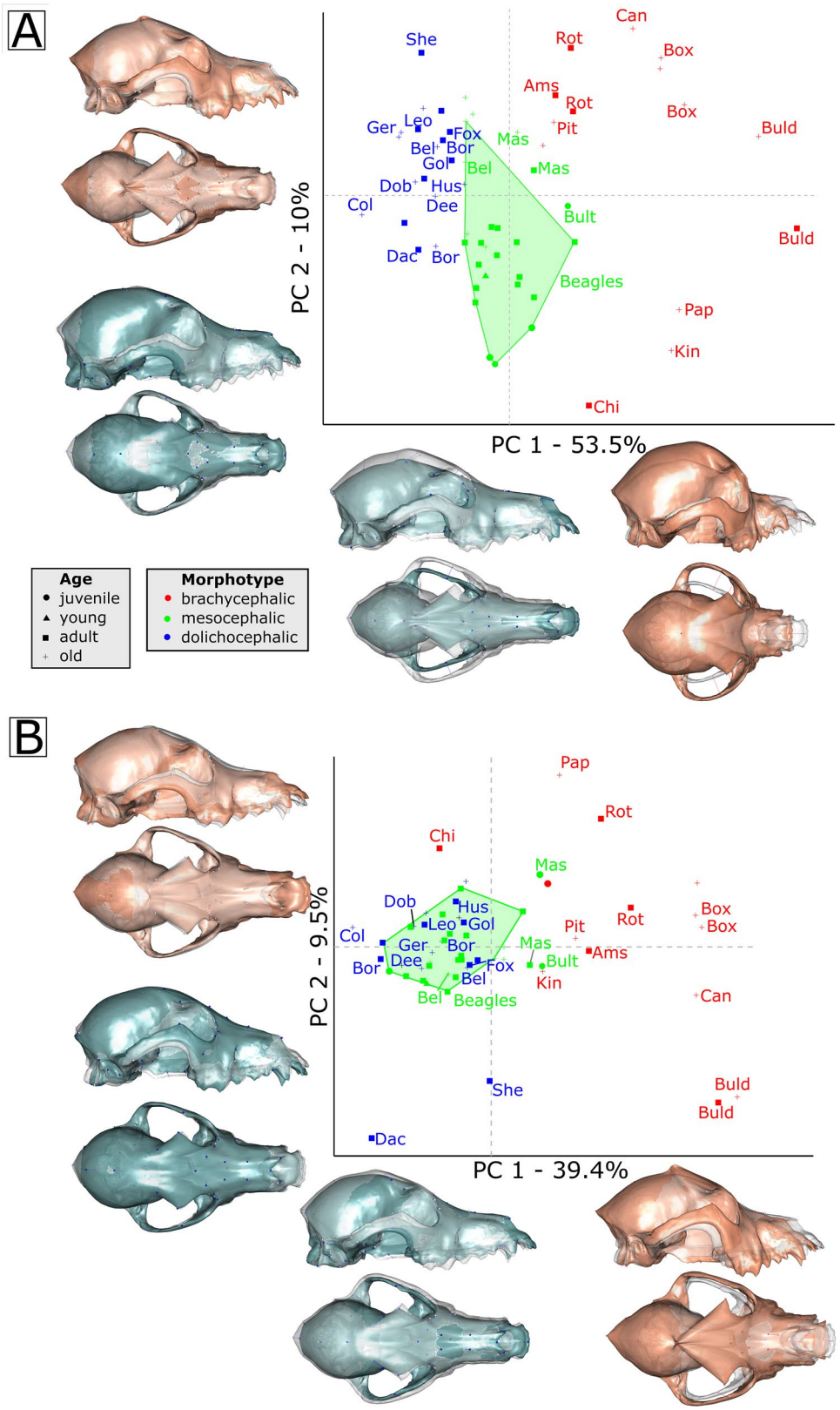

Fig. 2 Principal component analyses performed on cranial shapes (**a**) or allometry-free cranial shapes (**b**). The dorsal and lateral views of the shapes at the minimum of each axis are in blue. Shapes at the maximum of the axes are in red. Ages are indicated by different shapes and morphotypes are indicated by different colors. Beagles are located in the green area. *Ams* American Staffordshire terrier, *Box* Boxer, *Buld* Bulldog, *Bult* Bull terrier, *Chi* Chihuahua, *Can* Cane Corso, *Kin* Cavalier King Charles Spaniel, *Pap* Papillon, *Pit* Pitbull, *Rot* Rottweiler, *Mas* Mastiff, *Fox* Fox terrier, *Bel* Belgian Shepherd, *Bor* Border collie, *Col* Collie, *Dac* Dachshund, *Ger* German Shepherd, *Gol* Golden retriever, *Hus* Husky, *Leo* Leonberg, *She* Shetland sheepdog

(with long and narrow crania). Dogs on the right part of the scatterplot have crania with a very rounded and tall braincase, large zygomatic arches, and a short snout. They correspond mainly to molossoid dogs and to small brachycephalic dogs (Chihuahua, King Charles, and Papillon). Dogs to the left of the scatterplot have narrow crania with a lower braincase, a

Table 3 Results of the simple and multiple regressions performed on cranial shape (N = 47)

	Df	SS	MS	Rsq	F	Z	Pr(> SS)
Multiple regression							
Shape of the cranium (N = 47)							
Centroid size	1	0.10	0.11	**0.21**	21	3.7	0.001
Residual PCSA—temporal	1	0.050	0.050	**0.10**	10	3.3	0.001
Residual PCSA—masseter	1	0.037	0.037	**0.075**	7.6	3.0	0.005
Residual PCSA—pterygoid	1	0.026	0.026	**0.053**	5.3	2.7	0.001
Residual mass—temporal	1	0.034	0.034	**0.067**	6.8	3.7	0.001
Residual mass—masseter	1	0.044	0.044	**0.087**	8.8	4.5	0.001
Residual mass—pterygoid	1	0.011	0.011	**0.021**	2.1	2.4	0.036
Residuals	39	0.19	0.0050	0.39			
Allometry-free shape of the cranium (N = 47)							
Residual PCSA—temporal	1	0.028	0.028	**0.10**	6.6	4.2	0.001
Residual PCSA—masseter	1	0.018	0.018	**0.064**	4.2	3.3	0.005
Residual PCSA—pterygoid	1	0.016	0.016	**0.056**	3.7	3.2	0.002
Residual mass—temporal	1	0.020	0.020	**0.073**	4.8	3.9	0.001
Residual mass—masseter	1	0.026	0.026	**0.091**	6.0	4.6	0.001
Residual mass—pterygoid	1	0.0068	0.0068	0.024	1.6	1.5	0.076
Residuals	39	0.17	0.0042	0.59			
Shape of the mandible (N = 47)							
Centroid size	1	0.027	0.027	**0.091**	5.7	3.4	0.001
PCSA temporal	1	0.014	0.014	**0.048**	3.0	2.4	0.006
PCSA masseter	1	0.018	0.018	**0.060**	3.7	2.9	0.004
PCSA pterygoid	1	0.006	0.006	0.021	1.3	0.64	0.20
Mass temporal	1	0.012	0.012	**0.039**	2.4	2.2	0.016
Mass masseter	1	0.025	0.025	**0.085**	5.2	4.1	0.001
Mass pterygoid	1	0.0073	0.0073	0.025	1.5	1.6	0.10
Residuals	39	0.19	0.0048	0.63			
Allometry-free shape of the mandible (N = 47)							
PCSA temporal	1	0.0095	0.0095	**0.041**	2.2	2.1	0.018
PCSA masseter	1	0.013	0.013	**0.056**	3.0	3.0	0.003
PCSA pterygoid	1	0.0053	0.0053	0.023	1.2	0.61	0.27
Mass temporal	1	0.011	0.011	**0.047**	2.5	2.4	0.008
Mass masseter	1	0.015	0.015	**0.066**	3.5	3.5	0.002
Mass pterygoid	1	0.0066	0.0066	0.029	1.5	1.3	0.100
Residuals	39	0.17	0.0044	0.74			
Simple regressions							
Shape of the cranium							
Centroid size (N = 58)	1	0.11	0.11	**0.19**	13	4.2	0.001
Temporal, raw PCSA (N = 47)	1	0.028	0.028	0.056	2.7	1.8	0.051
Masseter, raw PCSA (N = 47)	1	0.027	0.027	0.053	2.5	1.6	0.069
Pterygoids, raw PCSA (N = 47)	1	0.031	0.031	**0.061**	2.9	1.9	0.045
Temporal, raw mass (N = 47)	1	0.033	0.033	**0.066**	3.2	2.0	0.043
Masseter, raw mass (N = 47)	1	0.034	0.034	**0.068**	3.3	2.0	0.038
Pterygoids, raw mass (N = 47)	1	0.036	0.036	**0.072**	3.5	2.1	0.027
Temporal, residual PCSA (N = 47)	1	0.050	0.050	**0.10**	5.0	2.8	0.004
Masseter, residual PCSA (N = 47)	1	0.079	0.079	**0.16**	8.4	3.4	0.001
Pterygoids, residual PCSA (N = 47)	1	0.093	0.093	**0.19**	10	3.6	0.001
Temporal, residual mass (N = 47)	1	0.10	0.10	**0.20**	12	3.7	0.001
Masseter, residual mass (N = 47)	1	0.14	0.14	**0.27**	17	4.2	0.001
Pterygoids, residual mass (N = 47)	1	0.15	0.15	**0.30**	20	4.4	0.001

Table 3 (continued)

	Df	SS	MS	Rsq	F	Z	Pr(> SS)
Allometry-free shape of the cranium							
Temporal, residual PCSA (N = 47)	1	0.028	0.028	**0.10**	5.0	3.6	0.001
Masseter, residual PCSA (N = 47)	1	0.038	0.038	**0.14**	7.1	4.2	0.001
Pterygoids, residual PCSA (N = 47)	1	0.047	0.047	**0.17**	9.0	4.7	0.001
Temporal, residual mass (N = 47)	1	0.053	0.053	**0.19**	11	5.0	0.001
Masseter, residual mass (N = 47)	1	0.066	0.066	**0.24**	14.3	5.5	0.001
Pterygoids, residual mass (N = 47)	1	0.075	0.075	**0.27**	17	6.1	0.001
Shape of the mandible							
Centroid size (N = 59)	1	0.037	0.037	**0.098**	6.2	4.2	0.001
Temporal, raw PCSA (N = 47)	1	0.033	0.033	**0.11**	5.6	3.8	0.001
Masseter, raw PCSA (N = 47)	1	0.043	0.043	**0.14**	7.5	4.3	0.001
Pterygoids, raw PCSA (N = 47)	1	0.038	0.038	**0.13**	6.7	4.1	0.001
Temporal, raw mass (N = 47)	1	0.040	0.040	**0.13**	7.0	4.1	0.001
Masseter, raw mass (N = 47)	1	0.049	0.049	**0.16**	8.8	4.5	0.001
Pterygoids, raw mass (N = 47)	1	0.045	0.045	**0.15**	8.1	4.3	0.001
Temporal, residual PCSA (N = 47)	1	0.014	0.014	**0.048**	2.3	2.1	0.029
Masseter, residual PCSA (N = 47)	1	0.027	0.027	**0.091**	4.5	3.4	0.001
Pterygoids, residual PCSA (N = 47)	1	0.023	0.023	**0.076**	3.7	3.1	0.001
Temporal, residual mass (N = 47)	1	0.027	0.027	**0.088**	4.5	3.3	0.001
Masseter, residual mass (N = 47)	1	0.043	0.043	**0.14**	7.6	4.4	0.001
Pterygoids, residual mass (N = 47)	1	0.045	0.045	**0.15**	8.0	4.5	0.001
Allometry-free shape of the mandible							
Temporal, residual PCSA (N = 47)	1	0.0095	0.0095	**0.041**	1.9	1.9	0.03
Masseter, residual PCSA (N = 47)	1	0.018	0.018	**0.076**	3.7	3.5	0.002
Pterygoids, residual PCSA (N = 47)	1	0.016	0.016	**0.067**	3.2	3.1	0.002
Temporal, residual mass (N = 47)	1	0.020	0.020	**0.082**	4.1	3.5	0.001
Masseter, residual mass (N = 47)	1	0.028	0.028	**0.12**	6.2	4.6	0.001
Pterygoids, residual mass (N = 47)	1	0.030	0.030	**0.13**	6.6	4.8	0.001

Significant results ($P < 0.05$) are indicated in bold

proportionally longer snout and narrow zygomatic arches. The beagles, represented by 20 crania, occupy the center of the scatter plot and extend along axis 2. This axis describes differences in size, the positioning of the zygomatic arches, and the width of the braincase, in particular the post-orbital constriction. In our sample, cranial shape is strongly allometric (Table 3, Fig. S1). The smallest dogs here correspond to small brachycephalic dogs: they have very rounded crania with wide zygomatic arches and a relatively short muzzle. The largest dogs of our sample have more dolichocephalic crania: they are relatively longer and narrower. However, these allometry patterns are strongly related to the constitution of our sample, because brachycephaly/mesocephaly/dolichocephaly do not depend on body size and each group may contain small, as well as medium or large breeds. The PCA performed on allometry-free shapes (Fig. 2b) still separated the brachycephalic (on the right) from the more dolichocephalic dogs (on the left). Molossoid dogs have wider zygomatic arches, a more voluminous neurocranium with more pronounced orbital processes, and a shorter snout, even for their size.

Drivers of Variation in Cranial Shape

The results of the Procrustes ANOVAs (Table 3) indicate that the shape of the cranium is driven by both centroid size and muscle architecture (the models explain 61% of the variation in cranial shape). According to the multiple regressions, 21% of the total variation in cranial shape is explained by size, while muscles explain 40.3% of the residual variation in shape. Both muscle masses and PCSAs are important drivers of cranial shape variation. The multiple Procrustes ANOVAs performed on allometry-free cranial shape and residual muscle masses and PCSAs (Table 3) also show significant result and muscles explain around 41% of the variation of non-allometric cranial shape.

The results of the simple regressions (whether on shape or allometry-free shapes) indicate that cranial shape is more strongly driven by muscle volume than by muscle PCSA. The relative mass of the temporal muscle explains 20% of the variation in cranial shape, while the relative volume of the masseter and pterygoid muscles explain 27 or 30% of

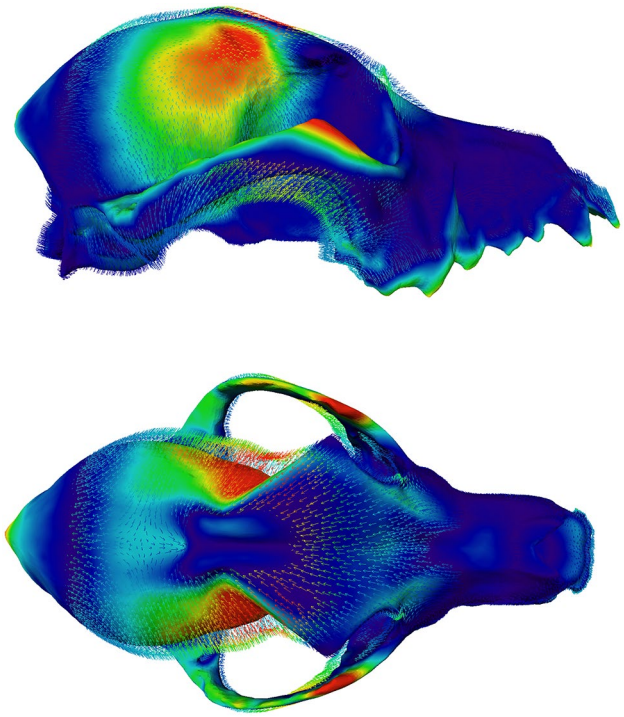

Fig. 3 Variation in cranial shape associated with variation in m. temporalis PCSA in lateral and dorsal views. The shape corresponding with the maximum of the PCSA is represented, and the arrows represent the deformation from the shape corresponding to the minimal PCSA to the shape corresponding to the maximal PCSA. Hotter colors indicate areas that show greater shape changes

the variation in cranial shape. Similar results and percentages are observed for the analysis with allometry-free cranial shape (Table 3). The visualisations highlight similar deformations associated with the temporal, masseter, and pterygoid muscles for both mass and PCSA. For all muscles, the zygomatic arches, the frontal bone, the sagittal crest, and the muzzle are the areas that are impacted the most (Fig. 3).

The ANOVAS and post-hoc tests performed on residual muscle data to compare brachycephalic, mesocephalic, and dolichocephalic dogs show that the masseter, temporal and pterygoid muscles are larger and more powerful in brachycephalic dogs than in meso or dolichocephalic dogs, relatively to their size ($P < 0.001$ for the masseter and pterygoid muscles; $P < 0.05$ for the temporal muscle). Differences between mesocephalic and dolichocephalic dogs were not significant.

Covariations Between Cranial and Mandibular Shape

The first PLS axis of the 2B-PLS between cranial and mandibular shape, accounting for 86% of the total covariance, is highly significant ($P < 0.001$) and indicates strong covariations (r-PLS = 0.82, Fig. 4a). The two axes are strongly dependent on the centroid sizes of the cranium and mandible, respectively (cranium: adjusted $R^2 = 0.15$, $P = 0.002$; mandible: adjusted $R^2 = 0.096$, $P = 0.012$). Molossoid dogs (large brachycephalic dogs) on the left part of the scatter plot have short and broad crania, with a short snout, a large neurocranium and wide zygomatic arches, associated to a ventrally curved mandibular body, with a large ramus and very developed coronoid, condylar and angular processes, and a deep masseteric fossa. On the opposite side of the scatterplot, we have the mesocephalic and dolichocephalic dogs. They have very elongated and narrow crania, with a smaller braincase, a longer snout and narrow zygomatic arches. This is associated with long and flat mandibles and smaller coronoid, condylar, and angular processes. The small brachycephalic dogs are located on the middle part of the scatterplot, the papillon being a little off-centre with respect to the main covariance axis. This covariation is not only linked with size variation, as the allometry-free shapes also show strong covariations (PLS 1 explains 79% of the total covariation, $P < 0.001$, r-PLS = 0.88, Fig. 4b). The deformations along the PLS axes are similar to those described for non allometry-free shapes, although the magnitude of the deformations is somewhat lower for the cranium.

Covariations Between Muscle Data and Cranial Shape

The results of the 2B-PLS are represented in Table 4. We observed significant covariations for all combinations. The covariations between cranial shape and raw PCSAs or between allometry-free cranial shape and residual PCSAs are stronger than the ones between cranial shape and residual PCSAs (shape: $Z = 1.97$, $P = 0.02$; allometry-free shape: $Z = 1.94$, $P = 0.03$). For the masses, the covariations are not significantly different. The visualisations are similar for the mass and the PCSA and the covariations are not significantly different ($P > 0.05$), although the coefficients tend to be higher for the 2B-PLS with masses.

Here we only describe the covariations between muscle masses and cranial shape. The scatterplots representing the first PLS axis reveals very strong covariations (mass: 96% of the total covariation, r-PLS = 0.9, $P = 0.025$; PCSA: 87% of the total covariation, r-PLS = 0.84, $P = 0.039$). All muscles loaded similarly reflecting the strong correlation between muscle groups. The covariatons between absolute muscle masses and the shape of the cranium (Fig. S2) are mainly driven by size (cranial shape: adjusted $R^2 = 0.58$, $P < 0.001$; muscle masses: adjusted $R^2 = 0.61$, $P < 0.001$). The covariations between shape and the residual masses (Fig. 5) indicate that molossoid dogs with a rounded neurocranium, larger zygomatic arches, shorter snouts, a more developed pterygoid process, and a more oblique cranium with more caudally located jugal teeth, have more developed muscles for

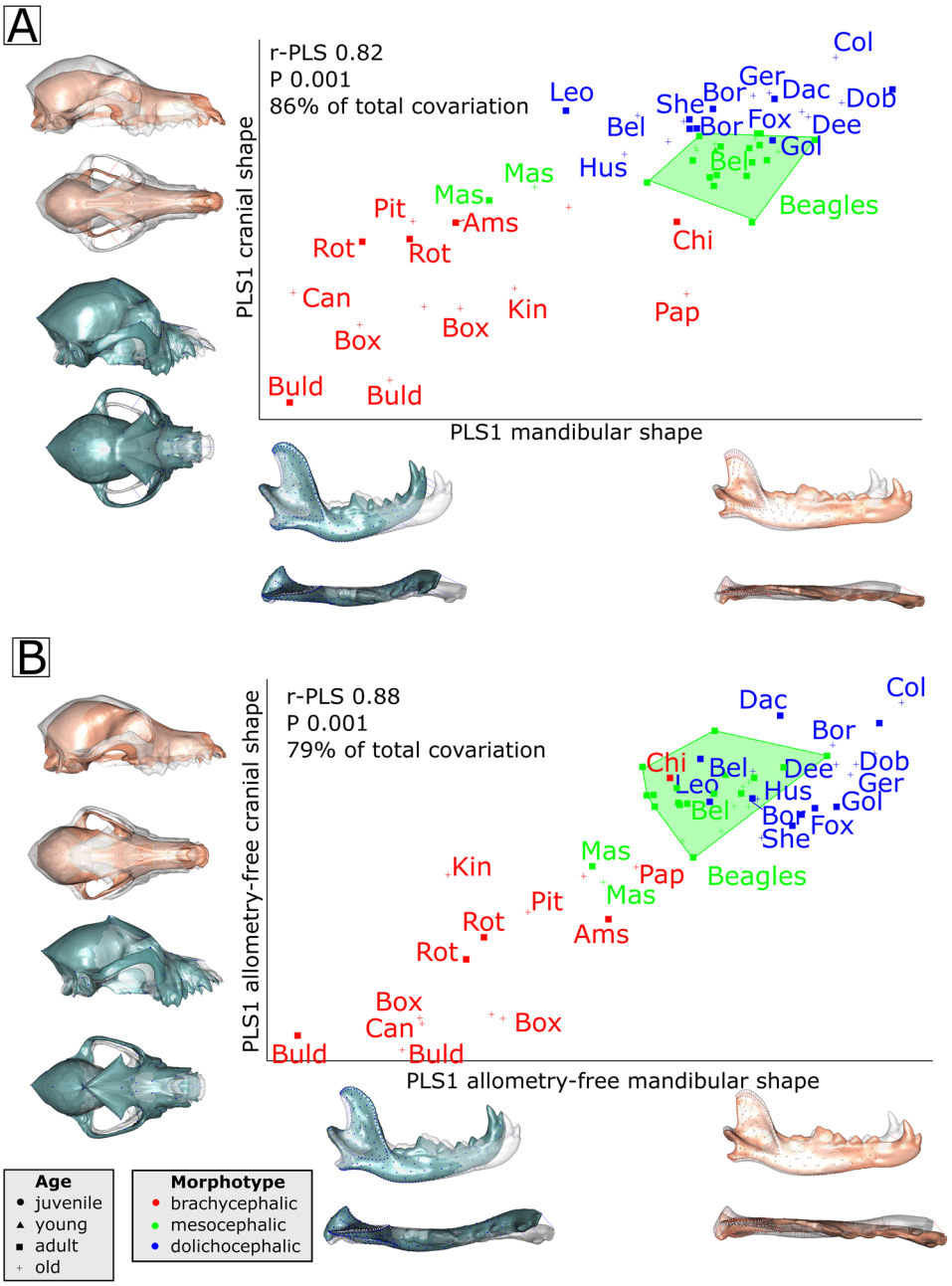

Fig. 4 2-Block Partial Least Square analyses between cranium and mandible shapes **(a)** or allometry-free cranium and mandible shapes **(b)**, with vectors and shapes at the minimum and maximum of the PLS axis. Illustrations represent the deformations from the consensus to the extreme of the axis in lateral and dorsal views. Ages are indicated by different shapes and morphotypes are indicated by different colors. Beagles are located in the green area. *Ams* American Staffordshire terrier, *Box* Boxer, *Buld* Bulldog, *Bult* Bull terrier, *Chi* Chihuahua, *Can* Cane Corso, *Kin* Cavalier King Charles Spaniel, *Pap* Papillon, *Pit* Pitbull, *Rot* Rottweiler, *Mas* Mastiff, *Fox* Fox terrier, *Bel* Belgian Shepherd, *Bor* Border collie, *Col* Collie, *Dac* Dachshund, *Ger* German Shepherd, *Gol* Golden retriever, *Hus* Husky, *Leo* Leonberg, *She* Shetland sheepdog

Table 4 Results of the 2B-PLS analyses on the shape of the cranium and the Log_{10}-transformed muscle mass or PCSA data

Muscle data	Shape–muscle data			Shape–residual data			Allometry-free shape–residual data		
	%CV	*P*	r-PLS	%CV	*P*	r-PLS	%CV	*P*	r-PLS
Mass	96	0.025	**0.90**	99	0.001	**0.74**	98	0.001	**0.83**
PCSA	87	0.039	**0.84**	96	0.001	**0.64**	93	0.001	**0.72**

Only the first PLS axis is reported. %coVar indicates the percentage of covariation explained by the axis of interest. r-PLS indicates the coefficient of covariation between the two variables. Significant results are indicated in bold

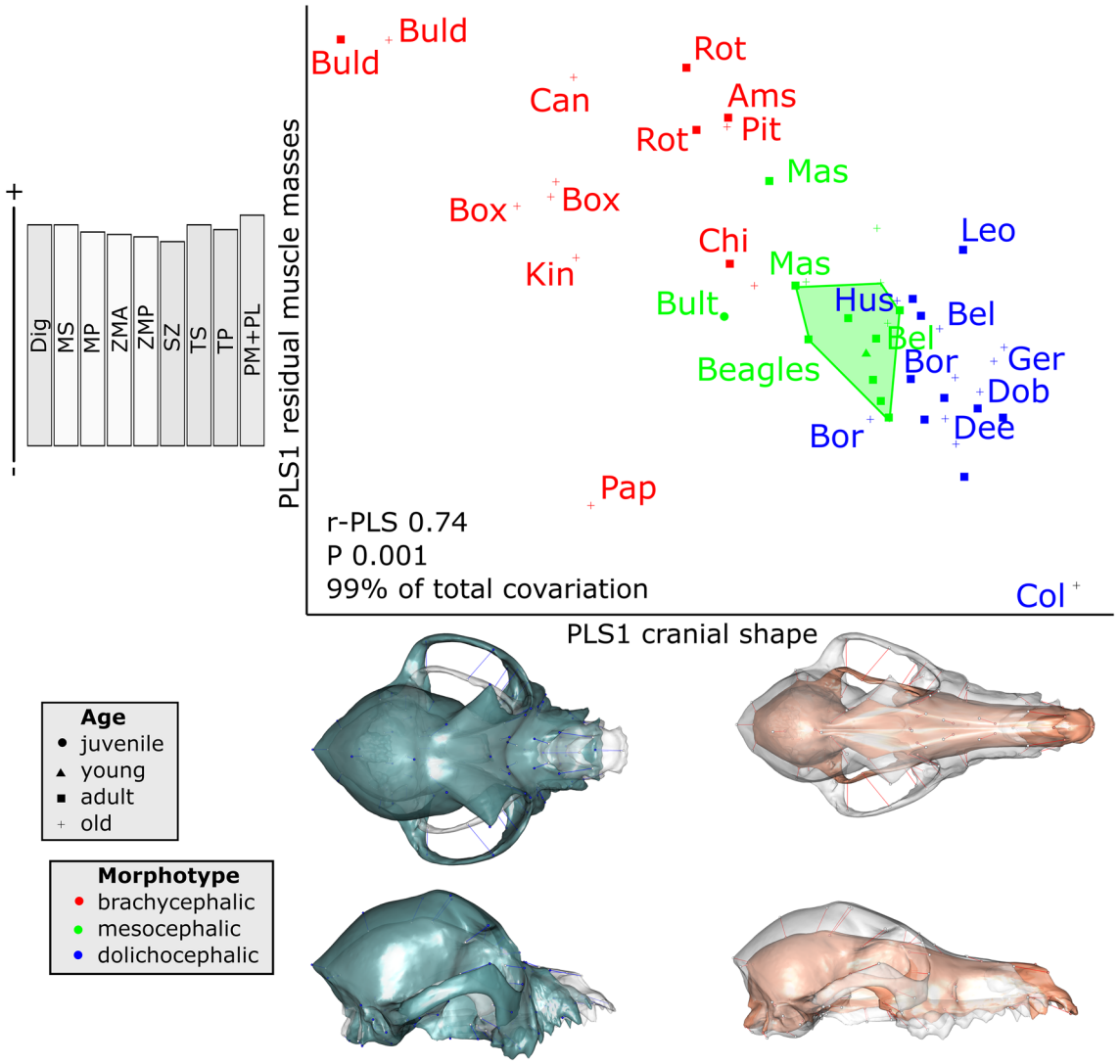

Fig. 5 2-Block Partial Least Square Analyses between cranial shape and the residual masses of the jaw muscles, with vectors and shapes at the minimum and maximum of the PLS axis. Illustrations represent the deformations from the consensus to the extreme of the axis in lateral and dorsal views. Ages are indicated by different shapes and morphotypes are indicated by different colors. Beagles are located in the green area. *Ams* American Staffordshire terrier, *Box* Boxer, *Buld* Bulldog, *Bult* Bull terrier, *Chi* Chihuahua, *Can* Cane Corso, *Kin* Cavalier King Charles Spaniel, *Pap* Papillon, *Pit* Pitbull, *Rot* Rottweiler, *Mas* Mastiff, *Fox* Fox terrier, *Bel* Belgian Shepherd, *Bor* Border collie, *Col* Collie, *Dac* Dachshund, *Ger* German Shepherd, *Gol* Golden retriever, *Hus* Husky, *Leo* Leonberg, *She* Shetland sheepdog, *Dig* M. digastricus, *MS* M. masseter pars superficialis, *MP* M. masseter pars profunda, *ZMA* M. zygomaticomandibularis pars anterior, *ZMP* M. zygomaticomandibularis pars posterior, *SZ* M. temporalis pars supra-zygomatica, *TS* M. temporalis pars superficialis, *TP* M. temporalis pars profunda, *PM+PL* M. pterygoideus pars medialis and lateralis

their size. More dolichocephalic dogs, on the right part of the scatterplot, which have straight, flat and narrow crania, with a long snout, a straight cranium, more cranially located jugal teeth and very small and narrow zygomatic arches, have less well-developed muscles. The beagles are grouped at the center of the scatterplot and the relations between cranial shape and the jaw muscles are rather homogenous. Visualisations of the 2B-PLS using allometry-free shape show similar patterns (Fig. S3).

Discussion

As previously observed (Drake et al. 2017) dog crania show an extraordinary variation in shape. Brachycephalic dogs with relatively big and rounded braincases, large zygomatic arches, and short snouts oppose dolichocephalic dogs that have long and narrow crania. Dogs from the same breed (beagles) also show variation in cranial shape but to a lesser degree. Yet, we found no significant effect of age which may be due to a bias in our sample and our age estimations. Males

and females did significantly differ in shape if we consider all breeds together. However, as our sample size is rather small (N = 32) and unbalanced we did not further explore the morphological traits related to sexual dimorphism. We did not have enough specimens of known sex (5) to test for sexual dimorphism in beagles specifically. In summary, cranial shape is allometric, and size explains more of the total variation in cranial shape ($R^2 = 0.21$) than mandible shape ($R^2 = 0.10$, Table 3).

We observed very strong covariations between mandible shape and cranial shape (rPLS = 0.81, $P = 0.001$; 85% of the total covariation, Fig. 4). We observed similar patterns of covariation as those previously described in the dog (Selba et al. 2019), other mammals (Cornette et al. 2013, 2015; Smith and Grosse 2016; Fabre et al. 2018; Penrose et al. 2020), and even in other tetrapods (Fabre et al. 2014). More robust and curved mandibles are associated with crania with a shorter snout and larger adductor chambers. The high coefficient of covariation is consistent with previously published data by Selba et al. (2019; r-PLS = 0.976; $P = 0.001$; 57 dogs). The slight differences are likely to be explained by the sample and to the lower number of landmarks used by Selba et al. (2019; 45 landmarks on the cranium and 17 on the mandible). This strong integration between the bony elements of the cranium suggests that the strong artificial selection upon morphological traits has not impacted the integrity of the jaw system. Possibly, the development of the overall system is under control of a limited set of key developmental genes assuring the integration between cranium and mandible. Moreover, Curth et al. (2017) showed that the greater skull shape diversity in dogs was not explained by less integrated skull modules and that the pattern of covariation in the cranium is similar to that observed in the wolf. Further studies focusing on the wolf and commensal canids might provide information about the impact of domestication in canids and test whether lower values of integration are associated with higher disparity across the modules in the cranium/mandible as has been documented in equids (Heck et al. 2018).

Cranial shape is also significantly impacted by the architecture of the muscles. Absolute muscle data explain less of the total variation in cranial shape than in mandibular shape (Table 3). This may be related to the implication of the cranium in numerous functions including the protection of the brain and the sensory organs, while the mandible is specialized towards mastication only. Unexpectedly, the covariations are stronger for the cranium compared to the mandible (mass: rPLS = 0.90 for the cranium and 0.74 for the mandible, Z-score = 2.45, $P = 0.007$; PCSA: r-PLS = 0.84 for the cranium and 0.73 for the mandible, Z-score = 2.02, $P = 0.02$). The covariations remain strong when the analyses are conducted on size-free data but the differences between the covariations between muscle architecture and the shape of the mandible and the cranium disappear (see also Brassard et al. 2020a; $P > 0.05$). The relative muscle data explain even more variation in cranial shape (40.3%) compared to mandible shape (22.4%, Table 3) and individual residual masses or PCSAs are better predictors of cranial shape than of mandibular shape. This may be explained by the differential contribution of the temporal and masseter muscle to the shape of the cranium and mandible and to their different contribution to the overall mass of the jaw adductors. The temporal muscle is the most voluminous muscle (Brassard et al. 2020a) and it covers the entire cranial vault while it inserts onto a small portion of the mandible (coronoid process). On the contrary, the masseter muscle is less voluminous, originates on a relatively small portion of the cranium (the lower portion of the zygomatic arch) but is attached to a large area on the mandibular ramus (the masseteric fossa). Both the masseter and temporal muscles may thus have distinct effects on the shape of the cranium or mandible, but it may be the attachment areas of the muscles that drive the covariations rather than the entire muscle mass per se. All this suggests that the cranium and the adductor muscles are a strongly integrated system.

Because of strong correlation between muscle masses/PCSAs, similar deformations are associated with all the muscles: the masseter, temporal, and pterygoid are acting jointly on overall cranial shape (Fig. 3). Dogs with the more voluminous or powerful muscles have a more caudally pronounced sagittal crest, a more marked postorbital constriction, and broader, stronger and more dorsally oriented zygomatic arches, bigger braincases, and reduced snouts (Figs. 5, S2, S3). The relative volume of the masseter explains 27% of the variation in cranial shape and impacts the shape of the zygomatic arch. The stiffness of the zygomatic arch in molossoid dogs suggests an adaptation to an increase in the relative proportion of applied muscle load due to the contraction of the more voluminous masseter muscle (Smith and Grosse 2016). The relative volume of the temporal drives the shape of the neurocranium, in particular the shape of the postorbital process and sagittal crest. The wide zygomatic arches determine the space available for the muscle to pass through.

Our results suggest that the mandible, the cranium, and the jaw adductors form a highly integrated system despite the intense artificial selection for very diverse head shapes. These strong connections are likely under genetic control, as suggested by studies on mice with muscle deficiencies. Vecchione et al. (2007, 2010) showed that mice with myostatin (a regulator of skeletal muscle growth) deficiency developed more brachycephalic craniofacial morphologies adapted to hypermuscularity, with significantly shorter and wider crania compared to controls (modifications in mandible shape were also observed). These modifications are consistent with our observations for the shape of the molossoid dogs that

have very voluminous muscles, even for their size. Spassov et al. (2017) also showed that mice with a congenital muscle dystrophy have a more flattened neurocranium with a more dorsally displaced foramen magnum. Our results also showed lower correlations and covariations of cranial shape with muscle PCSAs than with muscle mass. This suggests that volume constraints are likely the principal drivers of the observed covariation. The lower correlations between shape and PCSA may result from a decoupling between shape and bite force. Variation in PCSA (or bite force) may, in turn, correlate more to cortical bone thickness than to the overall shape of the cranium as demonstrated in other species or for other bones (Bouvier and Hylander 1981; Daegling and Hotzman 2003; Slizewski et al. 2013).

The low ratio of the number of individuals to the much higher number of variables is frequent in comparative morphology studies and may result in statistical biaises. It has been suggested that high correlations can possibly be observed in 2bPLS analyses even if the two blocks are completely independent when the sample size is smaller or similar to the number of variables (Mitteroecker and Bookstein 2007). However, more recent studies using simulated and empirical datasets have demonstrated that the potential issues related to the use of high-resolution three-dimensional data are unlikely to obscure genuine biological signal (Goswami et al. 2019). Moreover, to make sure that our results were not biased by the low sample size relative to the high number of landmarks, we performed parallel analyses with a subsample of 25 landmarks on the cranium and mandible. We obtained very similar results (in terms of *P*-values and coefficients of covariation) suggesting that our analyses are not biased by the number of landmarks used to describe shape variation.

Our study focused on the relations between the overall shape of the bones and muscles but did not allow to study the relations between muscle loads and bone histology, nor to evaluate the impact of changes in diet or muscle activity throughout life. The biomechanical interactions between muscle and bone have been investigated in some detail in mammals, showing that muscles act on bones throughout late ontogeny and adult life and that the bones of the cranium respond plastically to changes in masticatory function (Wolff 1986; Frost and Schönau 2000; Renaud et al. 2010; Herring 2011; Klingenberg and Navarro 2012; Blank 2014; Brotto and Bonewald 2015; Yamamoto et al. 2020). Diet is known to influence both muscle volume and cortical bone thickness in mammals (Bouvier and Hylander 1984; Herring 2011; Scott et al. 2014a, b) and even overall craniofacial shape (Stavros Kiliaridis et al. 1985; He and Kiliaridis 2003; Renaud et al. 2010; Anderson et al. 2014; Spassov et al. 2017). For example, rodents fed a soft food diet have a shorter and narrower face, and a shorter mandible with less pronounced bony processes compared to animals fed on a hard diet (Anderson et al. 2014; Kiliaridis et al. 1985). He and Kiliaridis (2003) further showed that ferrets fed a humid, soft diet have narrower crania with slenderer zygomatic arches and shorter and narrower coronoid process on the mandible, compared to ferrets fed with a dry, hard diet. Exercising also may have an influence on bone shape (Kiliaridis et al. 1995; Shirai et al. 2018; Thompson et al. 2001). Although few studies have focused on canids (but see Forbes-Harper et al. 2017; Liebman and Kussick 1965; Penrose et al. 2020; Wroe et al. 2007) these results suggest that diet may be an important driver of cranial shape variation in dogs as well, yet this remains to be investigated. Comparing domestic dogs with commensal or wild canids would further enable to better understand the impact of domestication on the interrelationships between muscles and bones of the jaw apparatus.

Conclusion

Our study assessed the impact of the extraordinary variation in cranial shape in domestic dogs on the interrelationships between bones and muscles. Our results show that the bony elements (cranium and mandible) and muscles form a highly integrated system in dogs. This supports the role of genes controlling both muscle and bone development, epigenetic effects driving the development of both muscles and bones (Iinuma et al. 1991), or the interaction between genetic mechanisms and plasticity. The strong integration of the masticatory apparatus consequently provides the possibility to infer the functional consequences of morphological changes in extinct taxa. Despite this strong integration, muscles explain relatively little of the overall shape variation in the cranium in domestic dogs. This raises the question of whether muscle architecture explains a higher proportion of the variation in shape in commensal or wild canids, and whether domestication has led to a change in the patterns of integration between form and function as suggested previously.

Acknowledgements We thank the Veterinary school ONIRIS-Nantes (France) and Anses (Nancy, France) for providing dog heads for dissection. We are grateful to Manuel Comte, Mickaël Godet and Frederic Lebatard for their help in managing specimens and their helpful discussions about the preparation of the skulls. We also thank Arnaud Delapré for his help with photogrammetry. We are very grateful to two anonymous reviewers for their comments and advice on an earlier version of the manuscript.

Funding This research was funded by the Ministère de l'Enseignement supérieur, de la Recherche et de l'Innovation.

Compliance with Ethical Standards

Conflict of interest The authors declare that they have no conflicts of interest.

References

Adams, D. C., & Collyer, M. L. (2016). On the comparison of the strength of morphological integration across morphometric datasets. *Evolution, 70*(11), 2623–2631. https://doi.org/10.1111/evo.13045.

Adams, D. C., & Collyer, M. L. (2017). Multivariate phylogenetic comparative methods: Evaluations, comparisons, and recommendations. *Systematic Biology, 67*(1), 14–31.

Anderson, M. J. (2001). A new method for non-parametric multivariate analysis of variance. *Austral Ecology, 26*(1), 32–46.

Anderson, M., & Braak, C. T. (2003). Permutation tests for multifactorial analysis of variance. *Journal of Statistical Computation and Simulation, 73*(2), 85–113.

Anderson, P. S., Renaud, S., & Rayfield, E. J. (2014). Adaptive plasticity in the mouse mandible. *BMC Evolutionary Biology, 14*(1), 1–9. https://doi.org/10.1186/1471-2148-14-85.

Barone, R. (2010). *Anatomie comparée des mammifères domestiques: Tome 1, Ostéologie* (5e édition.). Paris: Vigot.

Bell, A. F. (1965). Dental disease in the dog. *Journal of Small Animal Practice, 6*(6), 421–428. https://doi.org/10.1111/j.1748-5827.1965.tb04359.x.

Blank, R. D. (2014). Bone and muscle pleiotropy: The genetics of associated traits. *Clinical Reviews in Bone and Mineral Metabolism, 12*(2), 61–65. https://doi.org/10.1007/s12018-014-9159-4.

Bookstein, F. L. (1997). *Morphometric tools for landmark data: Geometry and biology*. Cambridge: Cambridge University Press.

Bouvier, M., & Hylander, W. L. (1981). Effect of bone strain on cortical bone structure in macaques (Macaca mulatta). *Journal of Morphology, 167*(1), 1–12. https://doi.org/10.1002/jmor.1051670102.

Bouvier, M., & Hylander, W. L. (1984). The effect of dietary consistency on gross and histologic morphology in the craniofacial region of young rats. *American Journal of Anatomy, 170*(1), 117–126. https://doi.org/10.1002/aja.1001700109.

Brassard, C., Merlin, M., Guintard, C., Monchâtre-Leroy, E., Barrat, J., Callou, C., et al. (2020a). How does masticatory muscle architecture covary with mandibular shape in domestic dogs? *Evolutionary Biology*. https://doi.org/10.1007/s11692-020-09499-6.

Brassard, C., Merlin, M., Guintard, C., Monchâtre-Leroy, E., Barrat, J., Bausmayer, N., et al. (2020b). Bite force and its relationship to jaw shape in domestic dogs. *Journal of Experimental Biology*. https://doi.org/10.1242/jeb.224352.

Brotto, M., & Bonewald, L. (2015). Bone and muscle: Interactions beyond mechanical. *Bone, 80*, 109–114. https://doi.org/10.1016/j.bone.2015.02.010.

Collyer, M. L., Sekora, D. J., & Adams, D. C. (2015). A method for analysis of phenotypic change for phenotypes described by high-dimensional data. *Heredity, 115*(4), 357.

Cornette, R., Baylac, M., Souter, T., & Herrel, A. (2013). Does shape co-variation between the skull and the mandible have functional consequences? A 3D approach for a 3D problem. *Journal of Anatomy, 223*(4), 329–336. https://doi.org/10.1111/joa.12086.

Cornette, R., Tresset, A., & Herrel, A. (2015). The shrew tamed by Wolff's law: Do functional constraints shape the skull through muscle and bone covariation? *Journal of Morphology, 276*(3), 301–309. https://doi.org/10.1002/jmor.20339.

Curth, S. (2018). Modularity and integration in the skull of *Canis lupus* (Linnaeus 1758): A geometric morphometrics study on domestic dogs and wolves, 78.

Curth, S., Fischer, M. S., & Kupczik, K. (2017). Patterns of integration in the canine skull: An inside view into the relationship of the skull modules of domestic dogs and wolves. *Zoology (Jena, Germany), 125*, 1–9. https://doi.org/10.1016/j.zool.2017.06.002.

Daegling, D. J., & Hotzman, J. L. (2003). Functional significance of cortical bone distribution in anthropoid mandibles: an in vitro assessment of bone strain under combined loads. *American Journal of Physical Anthropology, 122*(1), 38–50. https://doi.org/10.1002/ajpa.10225.

Drake, A. G., Coquerelle, M., Kosintsev, P. A., Bachura, O. P., Sablin, M., Gusev, A. V., et al. (2017). Three-dimensional geometric morphometric analysis of fossil canid mandibles and skulls. *Scientific Reports, 7*(1), 9508. https://doi.org/10.1038/s41598-017-10232-1.

Drake, A. G., & Klingenberg, C. P. (2008). The pace of morphological change: Historical transformation of skull shape in St Bernard dogs. *Proceedings. Biological sciences, 275*(1630), 71–76. https://doi.org/10.1098/rspb.2007.1169.

Drake, A. G., & Klingenberg, C. P. (2010). Large-scale diversification of skull shape in domestic dogs: Disparity and modularity. *The American Naturalist, 175*(3), 289–301. https://doi.org/10.1086/650372.

Dryden, I. L., & Mardia, K. V. (2016). *Statistical shape analysis: With applications in R*. New York: Wiley.

Ellis, J. L., Thomason, J. J., Kebreab, E., & France, J. (2008). Calibration of estimated biting forces in domestic canids: Comparison of post-mortem and in vivo measurements. *Journal of Anatomy, 212*(6), 769–780. https://doi.org/10.1111/j.1469-7580.2008.00911.x.

Ellis, J. L., Thomason, J., Kebreab, E., Zubair, K., & France, J. (2009). Cranial dimensions and forces of biting in the domestic dog. *Journal of Anatomy, 214*(3), 362–373. https://doi.org/10.1111/j.1469-7580.2008.01042.x.

Fabre, A.-C., Andrade, D. V., Huyghe, K., Cornette, R., & Herrel, A. (2014). Interrelationships between bones, muscles, and performance: biting in the lizard *Tupinambis merianae*. *Evolutionary Biology, 41*(4), 518–527. https://doi.org/10.1007/s11692-014-9286-3.

Fabre, A.-C., Perry, J. M. G., Hartstone-Rose, A., Lowie, A., Boens, A., & Dumont, M. (2018). Do muscles constrain skull shape evolution in strepsirrhines? *The Anatomical Record, 301*(2), 291–310. https://doi.org/10.1002/ar.23712.

Fau, M., Cornette, R., & Houssaye, A. (2016). Photogrammetry for 3D digitizing bones of mounted skeletons: Potential and limits. *Comptes Rendus Palevol, 15*(8), 968–977. https://doi.org/10.1016/j.crpv.2016.08.003.

Forbes-Harper, J. L., Crawford, H. M., Dundas, S. J., Warburton, N. M., Adams, P. J., Bateman, P. W., et al. (2017). Diet and bite force in red foxes: Ontogenetic and sex differences in an invasive carnivore. *Journal of Zoology, 303*(1), 54–63. https://doi.org/10.1111/jzo.12463.

Frost, H. M. (2001). From Wolff's law to the Utah paradigm: Insights about bone physiology and its clinical applications. *The Anatomical Record, 262*(4), 398–419. https://doi.org/10.1002/ar.1049.

Frost, H. M. (2003). Bone's mechanostat: a 2003 update. *The Anatomical Record Part A: Discoveries in Molecular, Cellular, and Evolutionary Biology: An Official Publication of the American Association of Anatomists, 275*(2), 1081–1101. https://doi.org/10.1002/ar.a.10119.

Frost, H. M., & Schönau, E. (2000). The" muscle-bone unit" in children and adolescents: a 2000 overview. *Journal of Pediatric Endocrinology and Metabolism, 13*(6), 571–590. https://doi.org/10.1515/JPEM.2000.13.6.571.

Goodall, C. (1991). Procrustes methods in the statistical analysis of shape. *Journal of the Royal Statistical Society: Series B (Methodological), 53*(2), 285–321.

Goswami, A., Watanabe, A., Felice, R. N., Bardua, C., Fabre, A.-C., & Polly, P. D. (2019). High-density morphometric analysis of shape and integration: The good, the bad, and the not-really-a-problem. *Integrative and Comparative Biology, 59*(3), 669–683. https://doi.org/10.1093/icb/icz120.

Gunz, P., Mitteroecker, P., & Bookstein, F. L. (2005). Semilandmarks in three dimensions. In D. E. Slice (Ed.), *Modern morphometrics in physical anthropology* (pp. 73–98). Boston: Springer.

He, T., & Kiliaridis, S. (2003). Effects of masticatory muscle function on craniofacial morphology in growing ferrets (*Mustela putorius* furo). *European Journal of Oral Sciences, 111*(6), 510–517. https://doi.org/10.1111/j.0909-8836.2003.00080.x.

Heck, L., Wilson, L. A. B., Evin, A., Stange, M., & Sánchez-Villagra, M. R. (2018). Shape variation and modularity of skull and teeth in domesticated horses and wild equids. *Frontiers in Zoology, 15*(1), 14. https://doi.org/10.1186/s12983-018-0258-9.

Herring, S. W. (2011). Muscle-bone interactions and the development of skeletal phenotype: Jaw muscles and the skull. *Epigenetics Linking Genotype and Phenotype in Development and Evolution., 13*, 201.

Iinuma, M., Yoshida, S., & Funakoshi, M. (1991). Development of masticatory muscles and oral behavior from suckling to chewing in dogs. *Comparative Biochemistry and Physiology. A, Comparative Physiology, 100*(4), 789–794. https://doi.org/10.1016/0300-9629(91)90293-l.

Kiliaridis, S., Engström, C., & Thilander, B. (1985). The relationship between masticatory function and craniofacial morphology: I. A cephalometric longitudinal analysis in the growing rat fed a soft diet. *The European Journal of Orthodontics, 7*(4), 273–283.

Kiliaridis, S., Tzakis, M. G., & Carlsson, G. E. (1995). Effects of fatigue and chewing training on maximal bite force and endurance. *American Journal of Orthodontics and Dentofacial Orthopedics: Official Publication of the American Association of Orthodontists, Its Constituent Societies, and the American Board of Orthodontics, 107*(4), 372–378. https://doi.org/10.1016/s0889-5406(95)70089-7.

Kim, S. E., Arzi, B., Garcia, T. C., & Verstraete, F. J. M. (2018). Bite forces and their measurement in dogs and cats. *Frontiers in Veterinary Science*. https://doi.org/10.3389/fvets.2018.00076.

Klingenberg, C. P., Barluenga, M., & Meyer, A. (2002). Shape analysis of symmetric structures: Quantifying variation among individuals and asymmetry. *Evolution, 56*(10), 1909–1920. https://doi.org/10.1111/j.0014-3820.2002.tb00117.x.

Klingenberg, C. P., & Navarro, N. (2012). Development of the mouse mandible. In J. Piálek, M. Macholán, P. Munclinger, & S. J. E. Baird (Eds.), *Evolution of the house mouse* (pp. 135–149). Cambridge: Cambridge University Press.

Liebman, F. M., & Kussick, L. (1965). An Electromyographic analysis of masticatory muscle imbalance with relation to skeletal growth in dogs. *Journal of Dental Research, 44*(4), 768–774. https://doi.org/10.1177/00220345650440042401.

Machado, F. A., Zahn, T. M. G., & Marroig, G. (2018). Evolution of morphological integration in the skull of Carnivora (Mammalia): Changes in Canidae lead to increased evolutionary potential of facial traits. *Evolution, 72*(7), 1399–1419. https://doi.org/10.1111/evo.13495.

Milella, L. (2009). Mandibular brachygnathism in dogs. *Companion. Animal, 14*(6), 29–35. https://doi.org/10.1111/j.2044-3862.2009.tb00382.x.

Mitteroecker, P., & Bookstein, F. (2007). The conceptual and statistical relationship between modularity and morphological integration. *Systematic Biology,56*(5), 818–836.

Mitteroecker, P., Gunz, P., Bernhard, M., Schaefer, K., & Bookstein, F. L. (2004). Comparison of cranial ontogenetic trajectories among great apes and humans. *Journal of Human Evolution, 46*(6), 679–698. https://doi.org/10.1016/j.jhevol.2004.03.006.

Parker, H. G., Kim, L. V., Sutter, N. B., Carlson, S., Lorentzen, T. D., Malek, T. B., et al. (2004). Genetic structure of the purebred domestic dog. *Science, 304*(5674), 1160–1164.

Penrose, F., Cox, P., Kemp, G., & Jeffery, N. (2020). Functional morphology of the jaw adductor muscles in the Canidae. *The Anatomical Record, 1*, 12. https://doi.org/10.1002/ar.24391.

Renaud, S., Auffray, J.-C., & de la Porte, S. (2010). Epigenetic effects on the mouse mandible: Common features and discrepancies in remodeling due to muscular dystrophy and response to food consistency. *BMC Evolutionary Biology, 10*, 28. https://doi.org/10.1186/1471-2148-10-28.

Roberts, T., McGreevy, P., & Valenzuela, M. (2010). Human induced rotation and reorganization of the brain of domestic dogs. *PLoS ONE, 5*(7), e11946. https://doi.org/10.1371/journal.pone.0011946.

Rohlf, F. J., & Corti, M. (2000). Use of two-block partial least-squares to study covariation in shape. *Systematic Biology, 49*(4), 740–753. https://doi.org/10.1080/106351500750049806.

Rohlf, F., & Slice, D. (1990). Extensions of the procrustes method for the optimal superimposition of landmarks. *Systematic Zoology, 39*, 40–59. https://doi.org/10.2307/2992207.

Schlager, S. (2012). *Sliding semi-landmarks on symmetric structures in three dimensions*. Présenté à the 81st annual meeting of the American Association of Physical Anthropologists, Portland, OR, Anthropology, University of Freiburg, Germany.

Schoenau, E. (2005). From mechanostat theory to development of the « Functional Muscle-Bone-Unit ». *Journal of Musculoskeletal and Neuronal Interactions, 3*, 232–238.

Scott, J. E., McAbee, K. R., Eastman, M. M., & Ravosa, M. J. (2014a). Teaching an old jaw new tricks: Diet-induced plasticity in a model organism from weaning to adulthood. *Journal of Experimental Biology, 217*(22), 4099–4107. https://doi.org/10.1242/jeb.111708.

Scott, J. E., McAbee, K. R., Eastman, M. M., & Ravosa, M. J. (2014b). Experimental perspective on fallback foods and dietary adaptations in early hominins. *Biology Letters, 10*(1), 20130789. https://doi.org/10.1098/rsbl.2013.0789.

Selba, M. C., Oechtering, G. U., Gan Heng, H., & DeLeon, V. B. (2019). The impact of selection for facial reduction in dogs: geometric morphometric analysis of canine cranial shape. *The Anatomical Record*. https://doi.org/10.1002/ar.24184.

Sharir, A., Stern, T., Rot, C., Shahar, R., & Zelzer, E. (2011). Muscle force regulates bone shaping for optimal load-bearing capacity during embryogenesis. *Development, 138*(15), 3247–3259. https://doi.org/10.1242/dev.063768.

Shirai, M., Kawai, N., Hichijo, N., Watanabe, M., Mori, H., Mitsui, S. N., et al. (2018). Effects of gum chewing exercise on maximum bite force according to facial morphology. *Clinical and Experimental Dental Research, 4*(2), 48–51. https://doi.org/10.1002/cre2.102.

Slizewski, A., Schönau, E., Shaw, C., & Harvati, K. (2013). Muscle area estimation from cortical bone. *The Anatomical Record, 296*(11), 1695–1707. https://doi.org/10.1002/ar.22788.

Smith, A. L., & Grosse, I. R. (2016). The biomechanics of zygomatic arch shape. *Anatomical Record, 299*(12), 1734–1752. https://doi.org/10.1002/ar.23484.

Spassov, A., Toro-Ibacache, V., Krautwald, M., Brinkmeier, H., & Kupczik, K. (2017). Congenital muscle dystrophy and diet consistency affect mouse skull shape differently. *Journal of Anatomy, 231*(5), 736–748. https://doi.org/10.1111/joa.12664.

Thompson, D. J., Throckmorton, G. S., & Buschang, P. H. (2001). The effects of isometric exercise on maximum voluntary bite forces and jaw muscle strength and endurance. *Journal of*

Oral Rehabilitation, 28(10), 909–917. https://doi.org/10.1111/j.1365-2842.2001.00772.x.

Vecchione, L., Byron, C., Cooper, G., Barbano, T., Hamrick, M. W., Sciote, J., et al. (2007). Craniofacial morphology in myostatin-deficient mice. *Journal of Dental Research, 86*(11), 1068–1072.

Vecchione, L., Miller, J., Byron, C., Cooper, G. M., Barbano, T., Cray, J., et al. (2010). Age-related changes in craniofacial morphology in GDF-8 (myostatin)-deficient mice. *The Anatomical Record: Advances in Integrative Anatomy and Evolutionary Biology, 293*(1), 32–41.

Wayne, R. K. (1986). Cranial morphology of domestic and wild canids: The influence of development on morphological change. *Evolution, 40*(2), 243–261. https://doi.org/10.1111/j.1558-5646.1986.tb00467.x.

Wiley, D. F., Amenta, N., Alcantara, D. A., Ghosh, D., Kil, Y. J., Delson, E., et al. (2005). Evolutionary morphing. In *VIS 05 IEEE visualization, 2005* (pp. 431-438). Présenté à VIS 05. IEEE Visualization. https://doi.org/10.1109/VISUAL.2005.1532826.

Wolff, J. (1986). *The law of bone remodelling*. Berlin: Springer.

Wroe, S., Clausen, P., McHenry, C., Moreno, K., & Cunningham, E. (2007). Computer simulation of feeding behaviour in the thylacine and dingo as a novel test for convergence and niche overlap. *Proceedings of the Royal Society B: Biological Sciences, 274*(1627), 2819–2828.

Yamamoto, M., Takada, H., Ishizuka, S., Kitamura, K., Jeong, J., Sato, M., et al. (2020). Morphological association between the muscles and bones in the craniofacial region. *PLoS ONE, 15*(1), e0227301. https://doi.org/10.1371/journal.pone.0227301.